



# The Shadow of a Spherically Accreting Black Hole

Ramesh Narayan<sup>1</sup> , Michael D. Johnson<sup>1</sup> , and Charles F. Gammie<sup>2,3</sup> <sup>1</sup>Center for Astrophysics | Harvard & Smithsonian, 60 Garden Street, Cambridge, MA 02138, USA; [marayan@cfa.harvard.edu](mailto:marayan@cfa.harvard.edu)<sup>2</sup>Department of Physics, University of Illinois at Urbana–Champaign, 1110 West Green Street, Urbana, IL 61801, USA<sup>3</sup>Department of Astronomy, University of Illinois at Urbana–Champaign, 1002 West Green Street, Urbana, IL 61801, USA

Received 2019 October 7; revised 2019 October 23; accepted 2019 October 25; published 2019 November 6

## Abstract

We explore a simple spherical model of optically thin accretion on a Schwarzschild black hole, and study the properties of the image as seen by a distant observer. We show that a dark circular region in the center—a shadow—is always present. The outer edge of the shadow is located at the photon ring radius  $b_{\text{ph}} \equiv \sqrt{27} r_g$ , where  $r_g = GM/c^2$  is the gravitational radius of the accreting mass  $M$ . The location of the shadow edge is independent of the inner radius at which the accreting gas stops radiating. The size of the observed shadow is thus a signature of the spacetime geometry and it is hardly influenced by accretion details. We briefly discuss the relevance of these results for the Event Horizon Telescope image of the supermassive black hole in M87.

*Unified Astronomy Thesaurus concepts:* [Black holes \(162\)](#); [Accretion \(14\)](#); [Strong gravitational lensing \(1643\)](#)

## 1. Introduction

Recently, the Event Horizon Telescope (EHT) obtained an ultra-high angular resolution image of the accretion flow around the supermassive black hole in M87 (The Event Horizon Telescope Collaboration 2019a, 2019b, 2019c, 2019d, 2019e, 2019f, hereafter EHT1–6). The image shows a bright ring of emission surrounding a dark interior (EHT4). The presence of such a dark central region was predicted by Falcke et al. (2000), who termed it the “shadow of the black hole.”

The shadow phenomenon is caused by gravitational light deflection—gravitational lensing—by the black hole. Lensing by a black hole was studied earlier in the context of an extended background source (Bardeen 1973) and for a geometrically thin, optically thick accretion disk (Luminet 1979). When the accretion flow produces radiation all around the black hole and the gas is optically thin to its own radiation, Falcke et al. (2000; see also Jaroszyński & Kurpiewski 1997) showed that lensing still produces a dramatic signature in the form of a shadow. They noted that the effect should be visible in Sagittarius A\*, the supermassive black hole at the center of our Galaxy, which is known to have a hot, optically thin accretion flow. Similar hot accretion flows are found around many supermassive black holes in the universe (Yuan & Narayan 2014), including the black hole in M87. All of these objects are natural candidates to reveal shadows in their images. The discovery by the EHT of a shadow-like feature in the image of M87 is thus verification of a fundamental prediction of general relativity in the regime of strong lensing.

As described in many previous studies, the outer edge of the shadow in a black hole image is located at the “photon ring,” which is the locus of rays that escape from bound photon orbits around the black hole to a distant observer. The photon ring, as defined here, was called the “apparent boundary” by Bardeen (1973) and the “critical curve” by Gralla et al. (2019). The latter authors questioned whether the EHT did in fact see a shadow surrounded by the photon ring in M87; they presented some models in which the details of the accretion flow seemed to matter more than any particular relativistic phenomenon such as the photon ring.

In this Letter we use a simple spherical model of black hole accretion to study the properties of the shadow and the photon ring. After some preliminaries in Section 2, we discuss in Section 3 a Newtonian model to clarify the notion of the shadow of an optically thin accretion flow in flat space. We then consider in Sections 4 and 5 two general relativistic models that use the Schwarzschild spacetime. We show that the shadow is a robust feature of these latter models and that its size and shape are primarily influenced by the spacetime geometry, and not by details of the accretion. We conclude in Section 6 with a discussion.

## 2. Terminology and Notation

We consider spherical accretion on a gravitating object of mass  $M$ . We use  $r_g = GM/c^2$  as our unit of length and  $c^2$  as our unit of energy. In the case of the Newtonian model (Section 3), we take the radius of the central mass to be  $2r_g$  and assume flat spacetime exterior to the surface. We also assume that any light rays that fall on the surface are completely absorbed.

For the general relativistic model (Sections 4 and 5), we consider a Schwarzschild black hole with spacetime metric

$$ds^2 = g_{tt} dt^2 + g_{rr} dr^2 + r^2 d\theta^2 + r^2 \sin^2 \theta d\phi^2, \quad (1)$$

where  $t$  is time,  $r$  is radius, and

$$g_{tt} = -\left(1 - \frac{2}{r}\right), \quad g_{rr} = \left(1 - \frac{2}{r}\right)^{-1}. \quad (2)$$

The horizon of the black hole is at  $r = 2$ , and the spacetime has an unstable circular “photon orbit” at radius

$$r_{\text{ph}} = 3. \quad (3)$$

A finely tuned photon at the photon orbit could, in principle, orbit the black hole an infinite number of times. However, since the orbit is unstable, any slight perturbation would cause the photon either to fall into the black hole or to escape to infinity. The photons that escape are seen by a distant observer to have an impact parameter  $b_{\text{ph}}$  with respect to the mass  $M$ , where

$$b_{\text{ph}} = \sqrt{27} \approx 5.2. \quad (4)$$

We refer to the circle in the observer’s sky with radius  $b_{\text{ph}}$ , centered on  $M$ , as the “photon ring.”

### 3. Newtonian Model

In Newtonian gravity, the potential energy of accreting gas varies with radius  $r$  as  $-1/r$ . Hence, we consider the following physically reasonable model of the power per unit volume  $P_N$  (erg cm<sup>-3</sup> s<sup>-1</sup>) radiated by the gas:

$$P_N(r) = \frac{1}{4\pi r^4}, \quad r \geq 2. \quad (5)$$

This is bolometric power, integrated over frequency. The total luminosity  $L_{\text{emit}}(r)$  emitted between radius  $r$  and infinity is

$$L_{\text{emit}}(r) = \int_r^\infty P_N(r') 4\pi r'^2 dr' = \frac{1}{r}, \quad (6)$$

i.e., proportional to the total potential energy drop from infinity to  $r$ , as is reasonable for accretion. The luminosity of an accretion flow depends of course on the mass accretion rate, so we ought to multiply  $P_N$  by a proportionality constant. However, under the fully optically thin conditions we consider in this Letter, none of the results depend on the constant, so for simplicity we ignore it. The emission coefficient per unit solid angle  $j_N$  (erg cm<sup>-3</sup> s<sup>-1</sup> ster<sup>-1</sup>) in this model is

$$j_N(r) = \frac{P_N(r)}{4\pi(\text{ster})} = \frac{1}{16\pi^2 r^4}, \quad r \geq 2. \quad (7)$$

Since the gas is optically thin, rays can travel arbitrarily large distances without being absorbed or scattered. However, not all of the emitted radiation escapes to infinity; any ray that intersects the “surface” of the central object at  $r = 2$  is absorbed and lost. In the Newtonian approximation considered in this section (flat space), rays travel in straight lines. Hence, for radiation emitted at radius  $r$ , the solid angle corresponding to rays that are lost is  $2\pi(1 - \cos\theta)$ , while that of rays that escape to infinity is  $2\pi(1 + \cos\theta)$ , where  $\sin\theta = 2/r$ . Thus, the net luminosity observed at infinity is

$$\begin{aligned} L_\infty &= \int_2^\infty j_N(r) 2\pi \left[ 1 + \sqrt{1 - \frac{4}{r^2}} \right] 4\pi r^2 dr \\ &= \frac{1}{4} + \frac{\pi}{16} \approx 0.45. \end{aligned} \quad (8)$$

We are interested in the image that a distant observer, located say on the  $z$ -axis, would see. For this, we compute the observed intensity  $I(b)$  (erg cm<sup>-2</sup> s<sup>-1</sup> ster<sup>-1</sup>) as a function of impact parameter  $b$ . For  $b \geq 2$ , this is given by

$$I(b) = \int_{-\infty}^\infty j_N(\sqrt{b^2 + z^2}) dz = \frac{1}{32\pi b^3}, \quad b \geq 2, \quad (9)$$

while for smaller impact parameters it is given by

$$\begin{aligned} I(b) &= \int_{\sqrt{4-b^2}}^\infty j_N(\sqrt{b^2 + z^2}) dz \\ &= \frac{1}{32\pi^2 b^3} \tan^{-1} \left( \frac{b}{\sqrt{4-b^2}} \right) - \frac{\sqrt{4-b^2}}{128\pi^2 b^2}, \quad b < 2. \end{aligned} \quad (10)$$

The black curve in Figure 1 shows the radial intensity profile  $I(b)$  for this Newtonian model, and the left panel in Figure 2 shows the two-dimensional image seen by a distant observer.

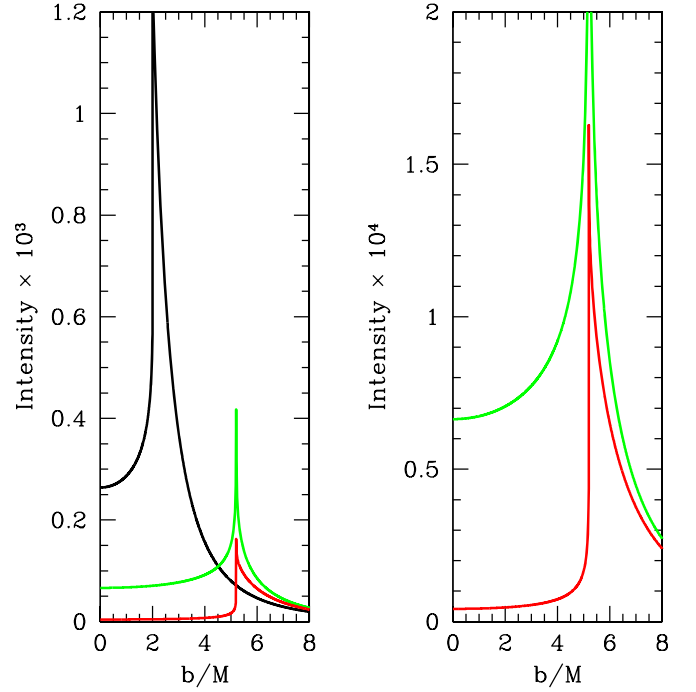


**Figure 1.** Left: the intensity profile  $I(b)$  as a function of the impact parameter  $b$  as seen by a distant observer for a spherically symmetric problem. The curves correspond to the Newtonian model (black), Schwarzschild spacetime with radiating gas at rest (green), and Schwarzschild spacetime with radially freefalling gas (red). Right: the two Schwarzschild models shown on an expanded vertical scale.

The intensity increases monotonically with decreasing impact parameter as  $1/b^3$ , until it reaches a maximum value equal to  $1/256\pi$  at the edge of the central object ( $b = 2$ ). Inside this critical impact parameter, the intensity drops suddenly by a factor of 2 since the line of sight terminates on the surface of the central mass and one no longer sees emission from the far side. It then continues to decrease inward and reaches a value of  $1/384\pi^2 \approx 2.64 \times 10^{-4}$  at  $b = 0$ . The intensity at the center is 4.7 times lower than the peak intensity at  $b = 2$ .

The dark region inside  $b = 2$  is what we term the “shadow” in the image. It is not a totally dark shadow with zero intensity, such as would be observed if the radiating gas were entirely behind the mass. Since we have radiating gas all around the mass, the image has some intensity even for lines of sight that intersect the surface of the central mass. Nevertheless, the shadow is a distinct feature. Its radius is well defined and could be measured by a distant observer with sufficiently good angular resolution. In this Newtonian problem, the shadow has a radius equal to 2.

### 4. Schwarzschild Spacetime with Gas at Rest

We now carry out a general relativistic analysis for a Schwarzschild black hole. In this section, we assume that the radiating gas is at rest. As in the Newtonian model, we assume that the net emitted luminosity between  $r$  and infinity is  $1/r$  (this is approximate, but is good enough for our purposes). To translate to the power per unit volume  $P_S(r)$  emitted in the proper frame of the gas, we note the following: (i) The proper length corresponding to the coordinate interval  $dr$  is  $\sqrt{g_{rr}} dr$ . (ii) Every unit of energy emitted in the local frame at  $r$  corresponds to  $\sqrt{-g_{tt}}$  units of energy at infinity. (iii) A time interval  $dt$  in the local frame corresponds to an interval  $dt/\sqrt{-g_{tt}}$  at infinity.

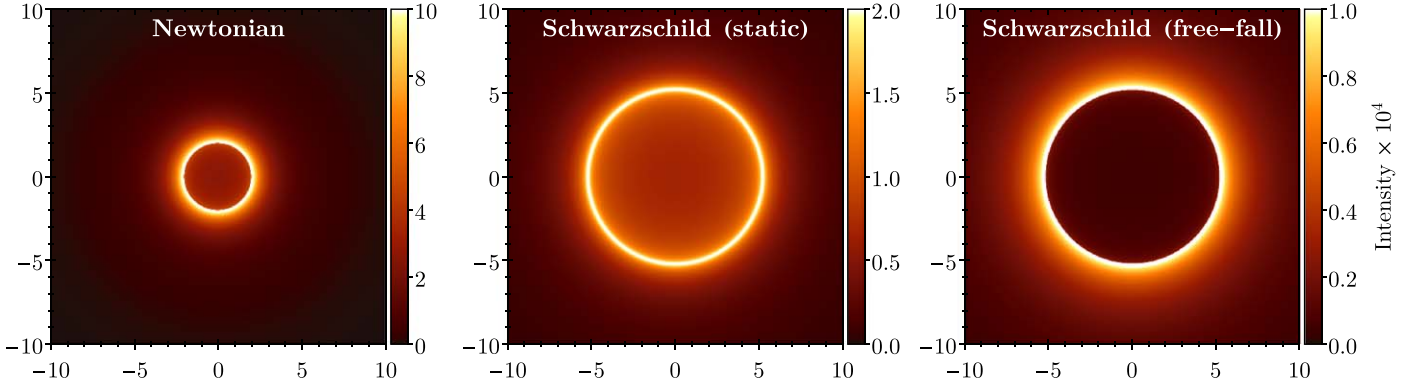


**Figure 2.** Image seen by a distant observer for the same models as in Figure 1: Newtonian model (left), Schwarzschild spacetime with gas at rest (middle), and Schwarzschild spacetime with radially infalling gas (right).

In view of these scalings, a natural choice for  $P_S$ , as well as the emission coefficient per unit solid angle  $j_S$ , is the following:

$$\begin{aligned} P_S(r) &= \frac{1}{|g_{tt}|\sqrt{g_{rr}}4\pi r^4} \\ &= \frac{1}{\left(1 - \frac{2}{r}\right)^{1/2}4\pi r^4} \\ &= 4\pi j_S(r), \quad r > 2. \end{aligned} \quad (11)$$

The precise functional form and the normalization are unimportant for what follows. The only virtue of the particular choice made here is that it enables easy comparison with the Newtonian problem discussed in Section 3. For instance, the net emitted luminosity in this model, measured at infinity, is

$$L_{\text{emit}}(r) = \int_r^\infty |g_{tt}|P_S(r')4\pi r'^2\sqrt{g_{rr}}dr' = \frac{1}{r}, \quad (12)$$

the same as in the Newtonian problem.

As before, only a fraction of the radiation emitted at any given  $r$  escapes to infinity. The solid angle of the escaping rays is equal to  $2\pi(1 + \cos\theta)$  for  $r \geq 3$  and  $2\pi(1 - \cos\theta)$  for  $r < 3$ , where  $\theta$  is given by<sup>4</sup> (we use the solution for which  $0 \leq \theta \leq \pi/2$ )

$$\sin\theta = \frac{3^{3/2}}{r}\left(1 - \frac{2}{r}\right)^{1/2}. \quad (13)$$

Counting only escaping rays, the net luminosity observed at infinity is

$$L_\infty = \frac{19}{60} \approx 0.32. \quad (14)$$

This is about 70% of the luminosity at infinity in the Newtonian problem. The reduced luminosity is because of gravitational deflection of light rays, which causes a larger fraction of the emitted radiation at any  $r$  to be captured by the black hole.

To calculate the intensity profile  $I(b)$ , we need a ray-tracing code (we use the code described in Zhu et al. 2015; Narayan et al. 2016). The result is shown by the green curves in Figure 1, as well as the 2D image in the middle panel of Figure 2.<sup>5</sup>

<sup>4</sup> This result can be obtained by using the fact that the critical rays that barely escape have specific angular momentum equal to that of the photon orbit:  $|k_\phi/k_{l,\text{crit}}| = |k_\phi/k_{l,\text{ph}}| = \sqrt{27}$ .

<sup>5</sup> The results presented here are most readily verified in a fully covariant treatment of radiative transfer using a separable plasma-frame emissivity  $j_S(r)\phi_\nu$ , where  $\int d\nu\phi_\nu = 1$ .

Qualitatively, the image in this general relativistic model is similar to the previous Newtonian image, with intensity increasing rapidly with decreasing  $b$ , reaching a peak at a finite  $b$ , and then dropping to lower values inside the peak. However, there are important differences. First, the peak is not at  $b = 2$ , the radius of the inner edge of the emitting gas, but is at the radius of the photon ring  $b_{\text{ph}}$ , which corresponds to the lensed image of the photon orbit  $r_{\text{ph}}$ . Thus, the shadow is significantly larger than in the Newtonian case. Second, the peak intensity at  $b = b_{\text{ph}}$  technically goes to infinity. This is because it is possible for rays with  $b = b_{\text{ph}}$  to make an infinite number of orbits around the black hole and to collect an arbitrarily large intensity<sup>6</sup>; because of numerical limitations, the actual computed intensity never goes to infinity. In any case, the divergence of the intensity at the photon ring is only logarithmic (Gralla et al. 2019; Johnson et al. 2019; but similar results go back many years, e.g., Darwin 1959; Luminet 1979), so the excess flux due to this divergence is small. Finally, the central intensity  $I(b = 0)$  is only 25% of that in the Newtonian problem:  $1/1536\pi^2 \approx 6.60 \times 10^{-5}$ .

## 5. Schwarzschild Spacetime with Infalling Gas

We now consider a more realistic model of an accreting Schwarzschild black hole: we allow the radiating gas to move in toward the black hole, as in a real accretion flow. In the spirit of our spherical model, we assume that the motion is purely radial. To make a specific choice for the radial velocity, we assume that the gas freefalls on to the black hole from infinity. Thus, we set  $u_r = -1$ , which corresponds to a velocity  $\beta = \sqrt{2/r}$  and Lorentz factor  $(1-2/r)^{-1/2}$  as measured by an observer at rest at radius  $r$ . For simplicity, we take the radiation power and emission coefficient, as measured in the rest frame of the infalling gas, to be the same as in Equation (11).

The ray-traced intensity profile  $I(b)$  corresponding to this model is shown by the red curves in Figure 1, and the 2D image seen by a distant observer is shown in the right panel in Figure 2. As before, the intensity increases toward smaller  $b$ , reaches nearly infinite intensity at  $b = b_{\text{ph}}$ , and then drops in the interior. A major new feature is that, because of inward gas motion, radiation that is emitted isotropically in the rest frame of the gas is beamed radially inward in the Schwarzschild frame. The beaming is especially large at small radii. Thus, a larger fraction of the radiation is lost into the black hole. The

<sup>6</sup> This is true under the assumed optically thin conditions. In reality, the intensity is limited to a finite maximum value because of optical depth effects.

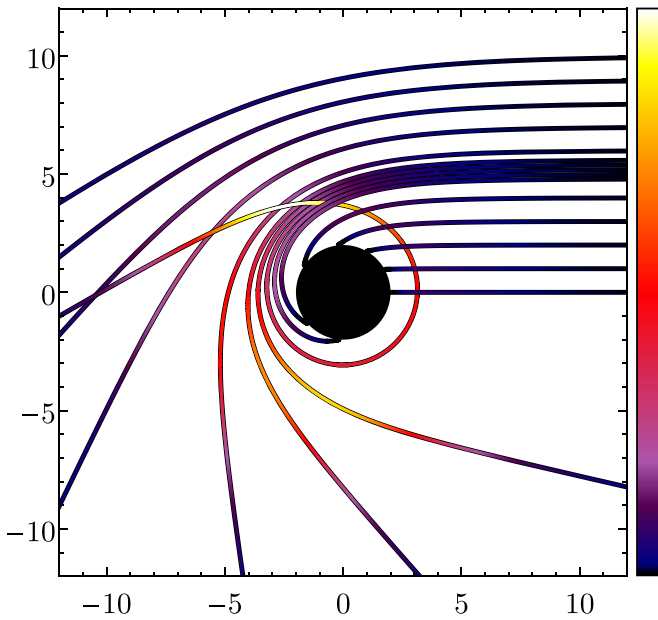


**Figure 3.** Example geodesics for a Schwarzschild black hole. Color indicates the effective emissivity along the ray for the case of radial infall, including Doppler effects. Rays are shown for impact parameters of  $b = 0$ – $10$  in steps of unity, with additional rays shown from  $b = 4.8$  to  $5.6$  in steps of  $0.2$  to highlight contributions near  $b_{\text{ph}}$ . The color scale is linear.

effect is particularly strong in the shadow region, which is now significantly darker than in the previous two models. For instance,  $I(b = 0)$  in this model is  $\approx 4.16 \times 10^{-6}$ , which is a factor  $\approx 16$  less than when the gas is at rest.

Figure 3 shows the emissivity contributions along representative null geodesics that travel toward an observer located to the far right of the plot. Doppler beaming causes portions of the geodesics that are moving in toward the black hole to be significantly brighter than those moving outward. Because rays with  $b < b_{\text{ph}}$  are always moving outward while those with  $b > b_{\text{ph}}$  always have both an inward and an outward segment, Doppler beaming causes a significant jump in the observed image brightness at the edge of the shadow (rays with  $b > b_{\text{ph}}$  are much brighter than equivalent rays with  $b < b_{\text{ph}}$ ). This explains why the shadow in the right panel in Figure 2 is so much deeper than that in the middle panel. For the same reason, as we show below, one obtains a deep shadow even if there is no emitting material at or near the photon orbit,  $r_{\text{ph}} = 3$ .

To the extent that, among the various spherical models considered in this Letter, the model with infalling gas comes closest to a radiatively inefficient accretion flow in a low-luminosity black hole, the shadow we compute in this section may be viewed as the best analog of the image observed in M87 (EHT4).

The most striking feature of the two relativistic model images in Figure 2 (middle and right panels) is the fact that the radius of the shadow is determined by the photon ring  $b_{\text{ph}}$ , which is a geometrical property of the spacetime. It is not determined by the inner radius of the radiating gas, which is located at the horizon,  $r_{\text{in}} = 2$ . Effectively, the spacetime geometry and lensing of photon trajectories erases details of the accretion flow at small radii, and imposes on the observed image a unique signature that reflects the properties of the spacetime.

To emphasize this point, we show in Figure 4 ray-traced images for six different models, all of which have radially

infalling gas in Schwarzschild spacetime. The top left panel corresponds to the model we just described, in which the gas radiates all the way down to the horizon:  $r_{\text{in}} = 2$ . In the remaining five models the emission is cutoff at progressively larger inner radii:  $r_{\text{in}} = 2.5, 3, 4, 5, 6$ . The first two of these models, in which the inner edge is inside the photon orbit  $r_{\text{ph}}$ , have images that are virtually indistinguishable from the initial model (they have slightly darker shadows, though it is hard to tell visually; see Figure 5). The remaining models, in which  $r_{\text{in}} > r_{\text{ph}}$ , show a weak feature in the image at the lensed location of  $r_{\text{in}}$ . However, the most prominent feature in all six models is the dark shadow in the middle. In each case the outer edge of the shadow is located at the radius of the photon ring  $b_{\text{ph}}$ . The spherical accretion model thus provides a class of counterexamples to the strong claim by Gralla et al. (2019) that the size of the shadow is very much dependent on the emission model.

The behavior of the image in the spherical model differs from that of geometrically thin disks, where the disk inner edge can have a prominent signature in the image, especially if the edge is outside the photon orbit (e.g., see Luminet 1979). However, the thin disk model is quite implausible for M87<sup>7</sup> or other low-luminosity galactic nuclei, which are known to contain geometrically thick hot accretion flows (Yuan & Narayan 2014).

## 6. Discussion

The main result of this Letter is that, for a spherically symmetric general relativistic (Schwarzschild spacetime) accretion model with optically thin gas, the concept of a shadow in the image is robust. The shadow is circular, and its outer edge is located at the photon ring radius  $b_{\text{ph}}$ , which is uniquely determined by the spacetime metric. The outer radius of the shadow does not depend on the details of the accretion flow. In particular, the location of the inner edge  $r_{\text{in}}$  of the radiating gas has very little effect. We demonstrate this in Figures 4 and 5, where we consider models from  $r_{\text{in}} = 2$  (the radius of the horizon) to  $r_{\text{in}} = 6$  (the radius of the innermost stable circular orbit). We find that the shadow has an identical size in all the models.

The intensity contrast between the interior of the shadow and the emission just outside  $b_{\text{ph}}$  depends on details of the accretion. The contrast is not large when the gas is stationary, but it is quite dramatic when the gas has a large inward radial velocity (compare the middle and right panels in Figure 2). Real accretion flows have inward motions, and the radial velocity tends to be large precisely at the radii of interest for shadow formation. Hence, the model with radially infalling gas is most appropriate for comparison with the image of M87.

Real accretion flows are not spherically symmetric. The hot accretion flow in Sagittarius A\*, M87, and most other galactic nuclei consists of a geometrically thick, quasi-spherical disk (Yuan & Narayan 2014), whose characteristics lie somewhere between the pure spherical model considered here and the geometrically thin disks considered in earlier work (e.g., Luminet 1979; Gralla et al. 2019).

Real black holes are also expected to have nonzero spin. We did not consider spin because the corresponding Kerr spacetime

<sup>7</sup> Gralla et al. (2019) give one such implausible model for M87, a thin disk terminating at the innermost stable circular orbit of a Schwarzschild black hole. This is their only example in which the “effective radius” of the image is significantly larger than the photon ring.



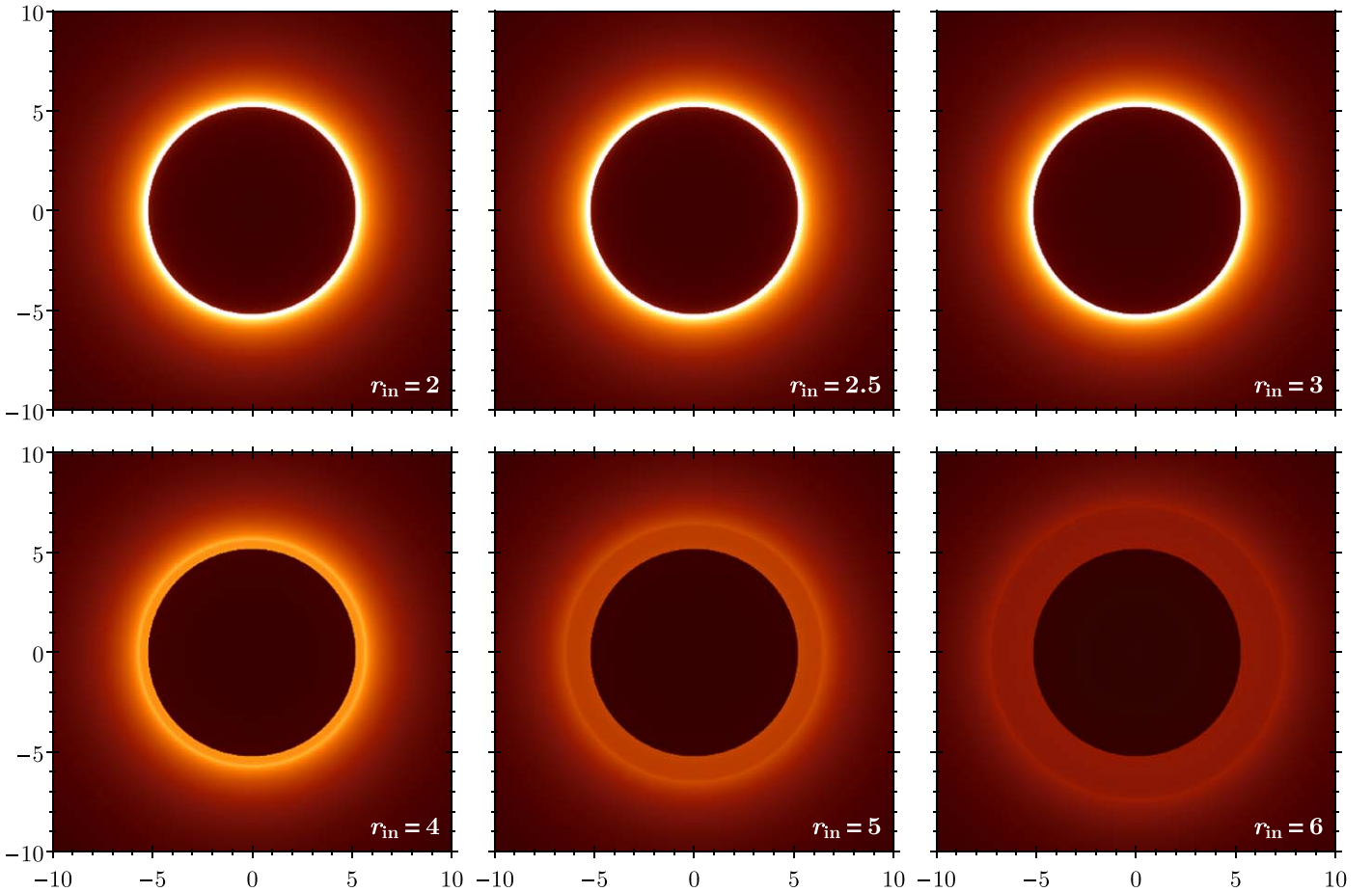


**Figure 4.** Image seen by a distant observer for radially infalling gas in Schwarzschild spacetime. The emission is cut off at different inner radii  $r_{\text{in}}$  in the various panels, extending from  $r_{\text{in}} = 2$  (top left) to  $r_{\text{in}} = 6$  (bottom right). All panels use a linear color scale from 0 to  $10^{-4}$  (see Figure 2).

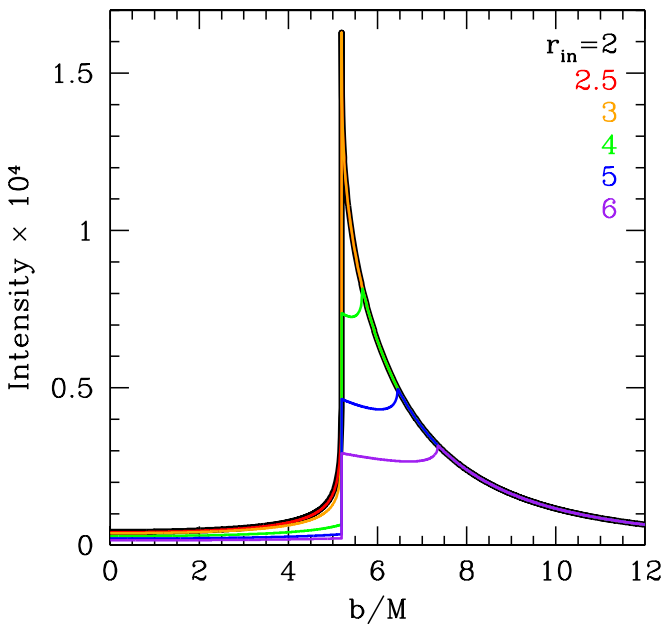


**Figure 5.** Intensity profile  $I(b)$  as a function of the impact parameter  $b$  for the models with radially infalling gas in Schwarzschild spacetime and varying emission cutoff radius  $r_{\text{in}}$ , as shown in Figure 4. In all cases, the radius of the shadow (the dark central region) is equal to  $b_{\text{ph}} \approx 5.2$ .

is not spherically symmetric, which complicates the model. Analysis of emission profiles of semi-analytic models of radiatively inefficient accretion flows around spinning black holes, beginning with Jaroszyński & Kurpiewski (1997), produce qualitatively similar results (see their Figure 3, noticing that the brightness profiles are averaged over position angle). More broadly, our simplified spherical model captures key features that also appear in state of the art GRMHD models (EHT5), whether they are spinning or not: (1) close in, the emissivity rises almost monotonically inward toward the horizon; (2) infall at  $r \sim 2GM/c^2$  leads to Doppler beaming of the emission toward the horizon, resulting in (3) low surface brightness on lines of sight that intersect the horizon: the shadow of the black hole.

An important observable signature that constrains non-spherical models is the presence of angular momentum in the accreting gas. This causes a Doppler asymmetry in the intensity distribution around the ring of emission outside the shadow. An azimuthal brightness asymmetry exceeding 2:1 is clearly seen in the observed image of M87 (EHT4) and also in model images based on GRMHD simulations (EHT5). Because M87 is viewed largely pole-on (the inclination angle is estimated to be  $17^\circ$ ; see Walker et al. 2018), the brightness asymmetry from rotation in a disk is relatively weak.

Another feature of real accretion that is not captured by our spherically symmetric model is the presence of outflows. Hot accretion flows tend to have inward accretion in more equatorial regions and outflows closer to the poles. Indeed, M87 has a powerful jet, which extends out to very large distances (Walker et al. 2018). At radii of interest to us ( $r \sim \text{few}$ ), the outward gas velocity in the polar regions is expected to be subrelativistic; in fact, if these radii are inside the “stagnation surface,” the gas may even be flowing in toward the black hole (e.g., Pu et al. 2017). Regardless, the Doppler boosting that causes the shadow to be so dark in our radial infall models (Figure 4) will be less pronounced or even absent in the polar regions. This might cause the contrast between the shadow and its exterior to be less pronounced (examples may be seen in EHT5).




Another practical matter is that observations never have the infinite angular resolution needed to identify precisely the edge of the shadow. With a finite resolution, one sees a blurred version of the image, where the emission ring one observes outside the shadow is a convolution of the intrinsic image intensity distribution  $I(b)$  and the point-spread function of the measurements. This often causes the peak of the ring to shift outward to a somewhat larger radius (by about 10%) than the photon ring radius  $b_{\text{ph}}$ . This effect and its uncertainties can be quantified using simulations, and EHT6 included it in the estimation and error budget for the mass of the black hole in M87.

Because our interest in this Letter is the shadow, we focused only on the role the photon ring plays as the location where the shadow terminates. Another property of the photon ring is that it is a place where the image intensity can become large. An enhancement of the observed intensity happens whenever there is radiating gas in the vicinity of the photon orbit  $r_{\text{ph}}$ , and the gas is optically thin. This effect is seen, for instance, in the green and red curves in Figure 1, in the three models with  $r_{\text{in}} = 2, 2.5, 3$  in Figure 5 (but not the other three models), and also in simulation images in EHT5. The integrated excess flux in the sharp intensity peak is not very large because the divergence is only logarithmic. However, the sharpness of the peak produces a strong and robust signature in Fourier space, opening up the possibility of making precise measurements of

the photon ring with very long baseline interferometry in space (Johnson et al. 2019).

The authors thank Avery Broderick, Alexandru Lupsasca, Dimitrios Psaltis, and Andrew Strominger for comments, and the referee for a number of useful suggestions. R.N. was supported in part by grants OISE-1743747 and AST-1816420 from the National Science Foundation (NSF). M.J. was supported in part by grants AST-1716536 from the NSF and GBMF-5278 from the Gordon and Betty Moore Foundation. C.G. was supported in part by grants AST-1716327 and OISE-1743747 from the NSF. This work was carried out at the Black Hole Initiative, Harvard University, which is funded by grants from the John Templeton Foundation and the Gordon and Betty Moore Foundation to Harvard University.

### ORCID iDs

Ramesh Narayan  <https://orcid.org/0000-0002-1919-2730>  
 Michael D. Johnson  <https://orcid.org/0000-0002-4120-3029>  
 Charles F. Gammie  <https://orcid.org/0000-0001-7451-8935>

### References

- Bardeen, J. M. 1973, in *Black Holes (Les Astres Occlus)*, ed. C. Dewitt & B. S. Dewitt (New York: Gordon and Breach), 215
- Darwin, C. 1959, *RSPSA*, 249, 180
- Falcke, H., Melia, F., & Agol, E. 2000, *ApJL*, 528, L13
- Gralla, S. E., Holz, D. E., & Wald, R. M. 2019, *PhRvD*, 100, 024018
- Jaroszynski, M., & Kurpiewski, A. 1997, *A&A*, 326, 419
- Johnson, M. D., Lupsasca, A., Strominger, A., et al. 2019, *SciA*, submitted (arXiv:1907.04329)
- Luminet, J.-P. 1979, *A&A*, 75, 228
- Narayan, R., Zhu, Y., Psaltis, D., & Sadowski, A. 2016, *MNRAS*, 457, 608
- Pu, H.-Y., Wu, K., Younsi, Z., et al. 2017, *ApJ*, 845, 160
- The Event Horizon Telescope Collaboration 2019a, *ApJL*, 875, L1, (EHT1)
- The Event Horizon Telescope Collaboration 2019b, *ApJL*, 875, L2, (EHT2)
- The Event Horizon Telescope Collaboration 2019c, *ApJL*, 875, L3, (EHT3)
- The Event Horizon Telescope Collaboration 2019d, *ApJL*, 875, L4, (EHT4)
- The Event Horizon Telescope Collaboration 2019e, *ApJL*, 875, L5, (EHT5)
- The Event Horizon Telescope Collaboration 2019f, *ApJL*, 875, L6, (EHT6)
- Walker, R. C., Hardee, P. E., Davies, F. B., Ly, C., & Junor, W. 2018, *ApJ*, 855, 128
- Yuan, F., & Narayan, R. 2014, *ARA&A*, 52, 529
- Zhu, Y., Narayan, R., Sadowski, A., & Psaltis, D. 2015, *MNRAS*, 451, 1661